Surface Plasmon Enhanced Fluorescence of Cationic Conjugated Polymer on Periodic Nanoarrays

Kirsty Leong,[†] Melvin T. Zin,[§] Hong Ma,[‡] Mehmet Sarikaya,[‡] Fei Huang,[‡] and Alex K.-Y. Jen*[,†,‡]

Departments of Chemistry and Materials Science and Engineering, University of Washington, Seattle, Washington 98195-2120, United States, and 3M Corporate Research Analytical Laboratory, 3M Center, St. Paul, Minnesota 55144, United States

ABSTRACT The fluorescence from conjugated polymer assembled onto lithographically fabricated gold nanoarrays using genetically engineered peptides as molecular linkers is studied. A 16-fold increase in the photoluminescence of the conjugated polymer is observed when assembled on the optimized nanostructures due to surface plasmon enhanced fluorescence. This is achieved using a water-soluble cationic conjugated polymer, poly[(9,9-bis(6′-((*N*,*N*,*N*-trimethylammonium)hexyl)-2,7-fluorene)-*co*-4,7-di-2-thienyl-2,1,3-benzothiadiazole] dibromide (PFDBT-N^+), systematically tuning the vertical distance of PFDBT-N^+ from the gold nanopillar surface using solid-specific peptide linkers and horizontally optimizing the localized surface plasmon resonance by varying the geometric arrangements of the patterned metal nanoarrays. The diameter and tip-to-tip spacing of the nanopillars along with vertically tuning the distance of PFDBT-N^+ from the nanopillar affected the observed fluorescence enhancements. The collective optical properties of conjugated polymers combined with the photonic properties of nanoparticles provide a new means in the development of metal enhanced hybrid nanomaterials for biotechnology.

KEYWORDS: hybrid nanostructure • metal-enhanced fluorescence • conjugated polymer • surface plasmon resonance

INTRODUCTION

Bio−nano hybrid systems result from the interfaces among life science, materials science, and biotechnology, and are a highly desirable composition because they offer high functionality and stability for a variety of practical applications (1−7). These hybrid nanosystems are composed of inorganic nanostructures, biomolecules, and organic molecules and have been shown to play an important role in photovoltaics (8), biomedicine (9), and sensors (10). In particular, research efforts are motivated by the unique physical properties of two classes of building blocks: inorganic nanostructures and fluorescent conjugated polymers. Inorganic nanostructures exhibit unique electronic, optical, and catalytic properties that can be used in nanoscale assemblies to alter the photophysical properties of nearby emitters (11−13). Meanwhile, fluorescent conjugated polymers (CPs) possess electrical, optical, and optoelectronic properties which can be tailored by rational molecular design and have the ability to amplify a chemical signal into a measured electrical or optical event (14). Hence, continuous efforts have been devoted in studying these combined building blocks for potential applications in biotechnology and nanoelectronics (15−18).

CPs are characterized by a delocalized electronic structure and can be used as highly responsive optical reporters for chemical and biological targets (14, 19). The molecular structure is composed of a series of conjugated segments or molecular units held in close proximity by the polymer backbone for electron delocalization. This collective behavior gives rise to optical enhancement or amplification if the low energy site consists of a reporter fluorophore. CPs have unique properties that are not exhibited by monomeric fluorophores such as amplified fluorescence through energy-harvesting, excellent transport of charges along the polymer chain, and strong UV−vis absorption (20). The efficient use of their light harvesting and optical amplification properties have been demonstrated to enhance sensing through Forster resonance energy transfer (21).

CPs modified with anionic or cationic functional groups have been explored for applications in electro-optic devices (22), biosensors (23), and drug delivery (24). They possess the properties of conjugated polymers and are water-soluble which is highly desirable and essential when interfacing with biological species such as proteins and deoxyribonucleic acid (DNA). Specifically, cationic conjugated polymers have been shown to be useful for DNA sequence detection based on electrostatic interactions where an environmental change at a single site affects the properties of the collective system producing large signal amplification (14a, 19, 25, 26). Of the various water-soluble CPs reported for biosensors, those synthesized from cationic poly(fluorene) (23b, 26−28) and

* Corresponding author. Email: ajen@u.washington.edu. Tel: (206) 543-2626. Fax: (206) 543-3100.
Received for review July 20, 2010 and accepted October 26, 2010
[†] Department of Chemistry, University of Washington.
[‡] Department of Materials Science and Engineering, University of Washington.
[§] 3M Corporate Research Analytical Laboratory.
DOI: 10.1021/am100635v

polythiophene derivatives (29) have been widely used for DNA sensing. Under the proper condition when CPs are interfaced with metal nanostructures to form hybrid assemblies, the amount of light absorbed and quantum yield of the CPs can be altered by the presence of the metal resulting in enhanced photoluminescence, a phenomenon known as metal enhanced fluorescence (30−33).

Metal enhanced fluorescence (MEF) attracts interest in the development of nanoassemblies for sensing devices (34), medical diagnosis (35), and opto-electronics (36). MEF occurs primarily due to near-field interactions of the excited state fluorophore with the local electric fields of metallic particles upon incident light. This interaction can enhance the emission of nearby fluorophores in several ways: through enhanced excitation (12), improved photostability, and/or better quantum yield (37). This effect is dependent on the nanoparticle's size, shape, and composition and the nanoparticle−dye separation (13, 38). Chen and coworkers have studied in detail the fluorescence intensity of dyes attached to silver nanoprisms, leading to the conclusion that the degree of spectral overlap between the plasmon resonance of the nanoparticle and the excitation and emission wavelengths of the emitter play an important role in MEF (30).

Current research interests in coupling plasmons in metal nanostructures have focused their efforts to investigate the interactions between metal nanoparticles and fluorescence dyes or quantum dots (QDs). Plasmon coupling between nanoparticles results in large electric field enhancements, which have the ability to amplify the fluorescence signal (39) and Raman scattering from adsorbed molecules (40). This concentration of the incident field does not occur homogeneously around the whole metallic nanostructure but exhibits local maxima such as the space between two neighboring nanoparticles (38, 41). Plasmon coupling of neighboring nanoparticles plays an important role in MEF in improving the sensitivity of detecting analytes at low concentrations. However, the interaction between nanoparticles and CPs has been less studied, and the ability to rationally design and controllably assemble CP-based hybrid nanoscale architectures still remains a challenge.

Here, we demonstrate a layer-by-layer self-assembly approach to combine optical amplification characteristics of CPs and large electric field enhancements of plasmonic nanoarrays for enhancing fluorescence emission. A 16-fold increase is observed in the brightness of poly[(9,9-bis(6′-((*N*,*N*,*N*-trimethylammonium)hexyl)-2,7-fluorene)-*co*-4,7-di-2-thienyl-2,1,3-benzothiadiazole] dibromide (PFDBT-N^+) when self-assembled at a distance of ∼18.50 nm from the metal surface and on 50 nm gold nanopillars with a tip-to-tip spacing of 50 nm. This hybrid nano-assembly was used to study the effects of vertical distance on the fluorescence of PFDBT-N^+ and spectral overlap between the plasmon resonance and the emission wavelength of PFDBT-N^+. This study differs from earlier works reported by Pompa et al. (42), Shankar et al. (43), and Zhang et al. (44) on plasmon enhanced systems. First, we studied the influence of localized surface plasmons on the placement of CPs to enhance the CPs emission. Second, we employed a protein strategy using genetically engineered peptides for the directed self-assembly of water-soluble cationic CPs onto metal surfaces at controlled distances. This offers a universal platform to generate hybrid nanostructures with high specificity and nanoscale precision. Third, we also optimize the plasmon-enhanced fluorescence by matching the resonant spectra of the nanoarray with the emission spectra of the emitter.

EXPERIMENTAL SECTION

Materials and Reagents. Sulfuric acid, hydrogen peroxide (30%), poly(methyl methacrylate), isopropyl alcohol, methyl-isobutylketone, streptavidin, chlorobenzene, ammonia hydroxide (28.0−30.0 % NH_3), 11-mercaptoundecyltri(ethylene glycol)-alcohol, and salmon DNA were purchased from Aldrich (St. Louis, MO) and used as received unless stated otherwise. Absolute (200 proof) ethanol was purchased from Aaper Alcohol and Chemical Company and used in preparation of thiol solutions. 1,4-Dibiotinylbutane was prepared by overnight refluxing a mixture of 1,4-butandiol and *d*-biotin (2.4 equiv) in toluene under nitrogen with 4-toluenesulfonic acid (0.1 equiv) as a catalyst. The crude product was purified in a silica gel column chromatography with an eluent, ethyl acetate/methanol (1:1), to afford a white solid (yield: 20%). The chemical structure of the compound was confirmed by ^{1}H NMR and mass spectrometry.

Poly[(9,9-bis(6′-((*N*,*N*,*N*-trimethyl-ammonium)hexyl)-2,7-fluorene)-*co*-4,7-di-2-thienyl-2,1,3-benzothiadiazole] dibromide (PFDBT-N^+) was synthesized in our laboratory. Details of the synthesis of PFDBT-N^+ are published elsewhere (45). The gold-binding polypeptide, referred to as *l*-AuBP2, with a peptide sequence WALRRSIRRQSY, was made using the standard Fmoc solid-phase peptide synthesis technique (46). Biotin (bio) was chemically linked to the *N*-terminus of the peptide to create a bifunctional bimolecular construct which serves as a binder for specific adsorption to the gold substrate as well as a receptor for controlling the self-assembly. Dulbecco's phosphate buffered saline (PBS) without calcium and magnesium was purchased from Invitrogen (Carlsbad, CA). Deionized (DI) water for rinsing was produced with a NANOpure Diamond purification unit (Barnstead International, Dubuque, IA) and had a resistivity of $\sim$15 MΩ cm^{-1}.

Gold Nanoarray Fabrication. Test grade (diameter, 100 mm; resistivity, 1−10 Ω/cm; thickness, 525 ± 50 μm) boron-doped Si (100) wafers were purchased from Silicon Sense (Nashua, NH). In preparation for electron-beam lithography (EBL), Si wafers were fractured into small substrates and cleaned using a two-step process: (i) piranha etch, 3:1 H_2SO_4/H_2O_2 (30%) for 1 h; (ii) base treatment, 5:1:1 $H_2O/NH_4OH/H_2O_2$ (30%) with sonication for 1 h. Thin films (110−140 nm) of polymethyl methacrylate (PMMA; 950kDa; diluted in chlorobenzene) resist were spin-coated on Si (001) substrates, annealed at 180°C on a hot plate for 2 min to improve the film uniformity, and then exposed to an electron beam at an accelerating voltage of 30k eV.

EBL was performed using a field emission scanning electron microscope (SEM; FEI Sirion, Hillsboro, OR) that has been equipped a nanolithography system. A nanometer pattern generation system (NPGS), developed by JC Nabity Lithography System (Bozeman, MT), was used to design and direct-write nanoarrays. After the electron-beam exposure, substrates were developed in a 1:3 mixture of methyl-isobutylketone/isopropanol (MIBK/IPA) at room temperature for ∼70 s and baked at 90°C in a vacuum oven for 30 min. The samples were checked using SEM to assess the integrity of nanopatterned PMMA films before the metallization process. Metals (5 nm of chromium and 50 nm of gold) were deposited onto nanopatterned PMMA films by electron-beam evaporation (SEC 6000, CHA Industries)

under a high vacuum with base pressure of ~1 × 10^{-6} Torr. The deposited thickness and deposition rate were measured by a quartz crystal microbalance (QCM). The deposition rate was maintained at ~0.1 nm s^{-1} to achieve high-quality gold nanostructures with smooth surfaces. In the lift-off step, gold nanoarrays were obtained by dissolving the PMMA resist in acetone overnight (~24 h).

Self-Assembly of Molecular Linkers. Biotin functionalized Bio-*l*-AuBP2 (100 μg/mL in PBS) is self-assembled onto the gold nanoarrays for 2 h, followed by the sequential attachment of spacer units using streptavidin (1 μM in DI water) and 1,4-dibiotinylbutane (1.0 mM ethanolic solution) for a reaction time of 35 min between each attachment. After each self-assembling step, the substrate was thoroughly rinsed using PBS, then DI water, and lastly ethanol.

Assembly of PFDBT-N^+. The EBL nanopatterned substrate functionalized with bio-*l*-AuBP2 and the spacer units, streptavidin and dibiotin, were immersed in another solution of bio-*l*-AuBP2 (100 μg/mL in PBS) for 35 min. After the bio-*l*-AuBP2 self-assembly, the substrate was rinsed with PBS, then DI water, and dried with N_2 gas. Then, the EBL nanopatterned substrate was immersed into DNA (1 mg/mL solution made using PBS) solution and allowed to self-assemble onto the molecular linkers for 30 min. After the DNA self-assembly, the substrate was rinsed with PBS and then DI water and dried with N_2 gas. A solution of PFDBT-N^+ was prepared in DI water to a working solution of 1 mg/mL. Then, the EBL nanopatterned substrate was immersed into the PFDBT-N^+ solution for 30 min, then thoroughly rinsed with DI water, and dried using N_2 gas.

Surface Characterization. Images were obtained from the EBL fabricated substrates using a FEI Sirion scanning electron microscope (SEM) at the University of Washington NanoTech User Facility at an accelerating voltage of 5 keV.

Atomic Force Microscopy. Images from experiments performed on gold substrates were carried out in air under ambient conditions (ca. 40−50% relative humidity, 25°C) on a Digital Instruments Nanoscope III Multimode atomic force microscopy (AFM; Veeco Inc., Santa Barbara, CA) using tapping mode at a scan rate of 0.5−1.0 Hz. Silicon cantilevers with spring constants ranging from 12 to 103 N/m were used. Image resolution was 512 × 512 pixels. Cross-sectional analysis was performed using an algorithm contained in the AFM software.

Measurement of Spacer Linkers. Silicon probes (Veeco Inc., Santa Barbara, CA) that have an effective radius of curvature of ~10 nm were used. The heights of molecular linkers were experimentally measured relative to the height of 11-mercaptoundecyltri (ethylene glycol)-alcohol (OEG-thiol purchased from Aldrich; 1 mM ethanolic solution) self-assembled monolayers (see Supporting Information Figure S1). This is accomplished by backfilling of linkers into 2 μm hole arrays generated by microcontact printing of OEG-thiol molecules, followed by cross-sectional profile analysis to measure the relative difference in heights between patterned OEG regions and linker regions.

Optical Microscope/Spectroscopy. Optical microscope/spectroscopy was performed using a Nikon TE-2000 inverted microscope fitted with a transmitted dark-field condenser and a 50× objective (Nikon Plan RT, NA 0.7, CC 0−1.2) with an intermediate 1.5× lens (total magnification 75×). The microscope output was either directed to a thermoelectrically-cooled color CCD camera (Diagnostic Instruments, FX1520) or a fiber optic cable (UV−vis transmission, Ocean Optics, Dunedin, FL) coupled to a portable charge coupled device spectrometer (USB2000, Ocean Optics). A standard tungsten halogen lamp was used for transmitted light dark-field illumination, and unpolarized white light illumination by a metal halide lamp (EXFO X-Cite 120) was used for epi-fluorescence illumination.

Measurements of Scattering Efficiency and Local Surface Plasmon Resonance Spectra. A lamp reference spectrum was obtained by measuring defocused, scattered white light from a kimwipe. A background spectrum was obtained by measuring the focused, scattered white light from the substrate to minimize noise. The fiber optic cable isolated the scattered light from each nanoparticle; this particle spectrum subtracted out from the background spectrum and divided by the lamp reference spectrum gave the scattering efficiency (and local surface plasmon resonance, LSPR, peak).

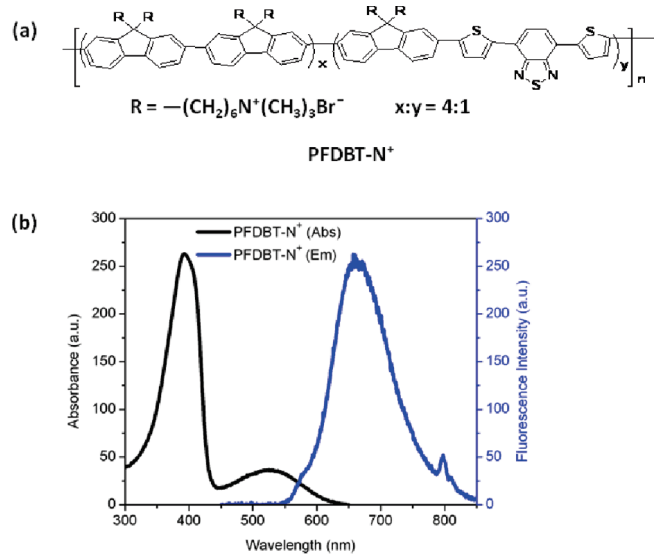

FIGURE 1. (a) Chemical structure of PFDBT-N^+. (b) Absorbance (black) and fluorescence emission (blue) spectra of a 1 mg/mL PFDBT-N^+ solution prepared in DI water.

Fluorescence Measurements. We obtained fluorescence intensities for each nanoarray by imaging the substrates with a 405 ± 20 nm excitation filter, 590 nm dichroic mirror, and 640 ± 40 nm emission filter. The filter set, purchased from Chroma Technology Corp (Rockingham, VT), reduced the background signal to less than 1% of the sample signal.

RESULTS AND DISCUSSION

Using a peptide mediated layer-by-layer self-assembly approach, we study the plasmon coupling effects on PFDBT-N^+ nanoarrays. PFDBT-N^+ is a water-soluble polyfluorene-based electrolyte with an absorption and emission maximum of 520 and 640 nm, shown in Figure 1a,b, respectively (45). The shoulder peak at 800 nm is due to spectral leak from the filter cube. Twelve different geometric arrangements of gold nanoarrays are fabricated to examine the dependence of spectral overlap between the plasmon resonance and the emission wavelength of PFDBT-N^+ on enhancing PFDBT-N^+ emission.

Fabrication and Optical Properties of Gold Nanoarray. EBL is used to fabricate 12 different geometric arranged gold nanoarrays, shown in Figure 2. At a constant height of 50 nm, gold nanoarrays of three varying diameters (D = 50, 100, 200 nm) were periodically ordered at four tip-to-tip spacings (d_{tt} = 50, 100, 150, 200 nm). The gold nanoarrays exhibit strong localized surface plasmon resonances that vary with both the diameter and tip-to-tip spacing of the gold nanopillars. The strong scattering of light reveals large field enhancement from the collective oscillation of the surface plasmons in noble metal nanostructures. The scattering spectra of the gold nanoarray show plasmon resonances ranging from 600 to 950 nm (Figure 3). The

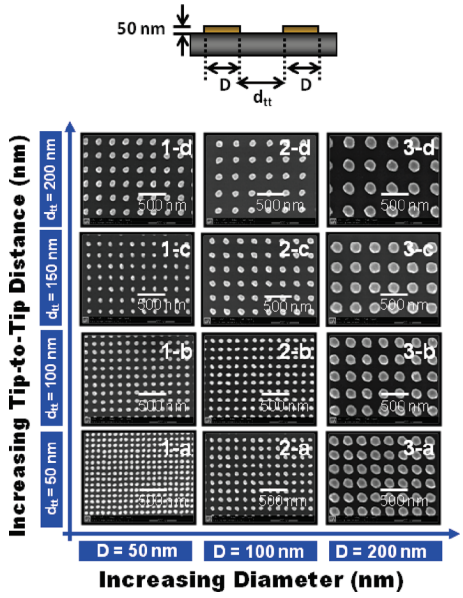

FIGURE 2. SEM image of gold nanoarrays in 12 geometric arrangements. The height was kept constant at 50 nm. The diameter (D) varied from 50 nm (1-a to 1-d) to 100 nm (2-a to 2-d) to 200 nm (3-a to 3-d). The tip-to-tip distances (d_{tt}) varied from 50 nm (a) to 100 nm (b) to 150 nm (c) to 200 nm (d).

plasmon resonance band of gold nanoarray is red-shifted from the plasmon resonance of a single gold nanoparticle which typically occurs around 520 nm (47). For a given diameter, the LSPR peak red-shifts as the d_{tt} distance increases from 50 to 200 nm. Similarly, when the nanopillar increases in diameter, the LSPR peak broadens and shifts to a longer wavelength. The variable ranges of LSPR peaks are favorable for observing the spectral overlap dependence between the LSPR of the nanoarray and the emission wavelength of PFDBT-N^+.

Efforts to model the experimental observations of electromagnetic-scattering on the gold nanopillars were employed using discrete dipole−dipole approximation with an analytical model tailored to describe periodic 1D and 2D array structures. The model is in agreement with the experiment observations that the dipole-plasmon resonance of the array is blue shifted with decreasing d_{tt} due to the long-range and retarded diffractive coupling of individual particle dipole moments. This behavior typically occurs when $D \geq 100$ nm, which is the regime of our observations. Details of the modeling and calculations have been published elsewhere (47).

Assembly of PFDBT-N^+ on Gold Nanoarrays. A peptide mediated layer-by-layer approach is used to assemble and vertically tune the distance of PFDBT-N^+ onto gold nanoarrays (Scheme 1). Spacer units composed of genetically engineered polypeptides for inorganic surfaces (GEPIs), biotin−streptavidin, and DNA are used to electrostatically bind PFDBT-N^+ onto the gold nanopillars at controlled distances. GEPIs offer several advantages because of their material specific biomolecular recognition, and potential bifunctional binding to inorganic solid surfaces (49). The GEPI used is a 12 amino acid gold binding polypeptide sequence (*l*-AuBP2 =WALRRSIRRQSY) containing a biotin

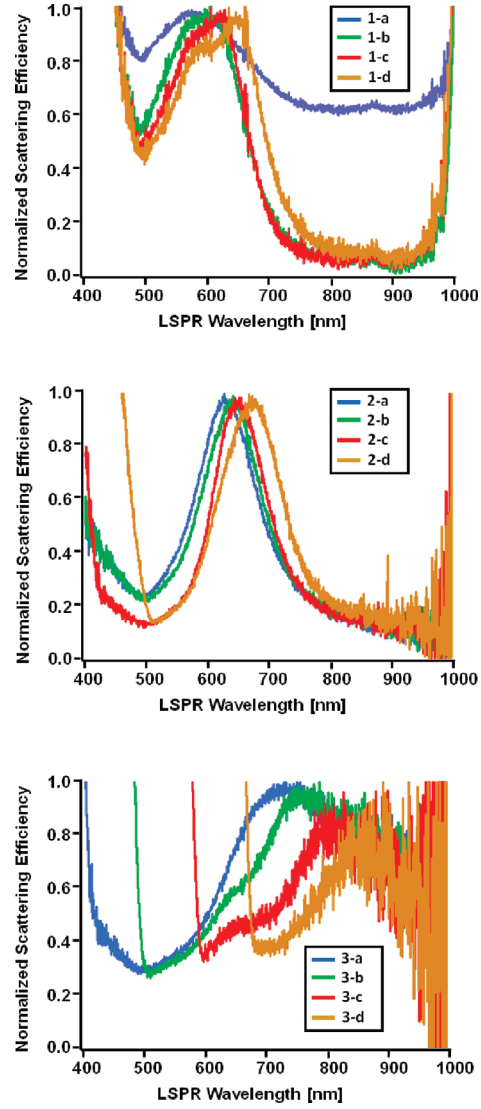

FIGURE 3. Scattering efficiency spectra of gold nanoarrays show distinct optical properties for each diameter and interparticle spacing. The top spectra correspond to $D = 50$ nm nanopillars; middle spectra correspond to $D = 100$ nm, and bottom spectra correspond to $D = 200$ nm. Blue colored spectra correspond to $d_{tt} = 50$ nm (1-a; 2-a; 3-a); green colored spectra correspond to $d_{tt} = 100$ nm (1-b; 2-b; 3-b); red colored spectra correspond to $d_{tt} = 150$ nm (1-c; 2-c; 3-c); gold colored spectra correspond to $d_{tt} = 200$ nm (1-d; 2-d; 3-d).

group on the N-terminus of the peptide chain (46). In addition, because the peptide sequence contains four arginine residues, *l*-AuBP2 has a +4 charge and, thus, can interact and self-assemble DNA through electrostatic interactions. DNA carries a negative charge because of the phosphate backbone and has been shown to interact with cationic conjugated polymers (50). A peptide-mediated approach allows for the placement of PFDBT-N^+ at three well-defined distances from the metal surface (CP−metal distance ~8.20, ~12.75, and ~18.50 nm). Details for the assembly and characterization of PFDBT-N^+ nanoarrays are described in the Supporting Information.

Photoluminescence of PFDBT-N^+ Nanoarray. The PFDBT-N^+ emission was measured at CP−metal distances of ~8.20, ~12.75, and ~18.50 nm (Figure 4). Self-assembled PFDBT-N^+ formed a closed-packed and optically

Scheme 1. Schematic Representation of the Peptide Mediated Self-Assembly of PFDBT-N$^+$ on the Gold Nanoarrays

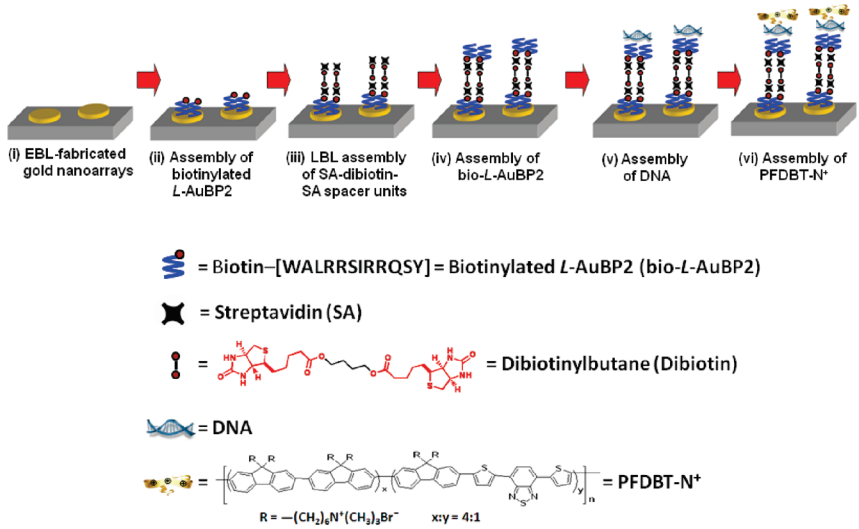

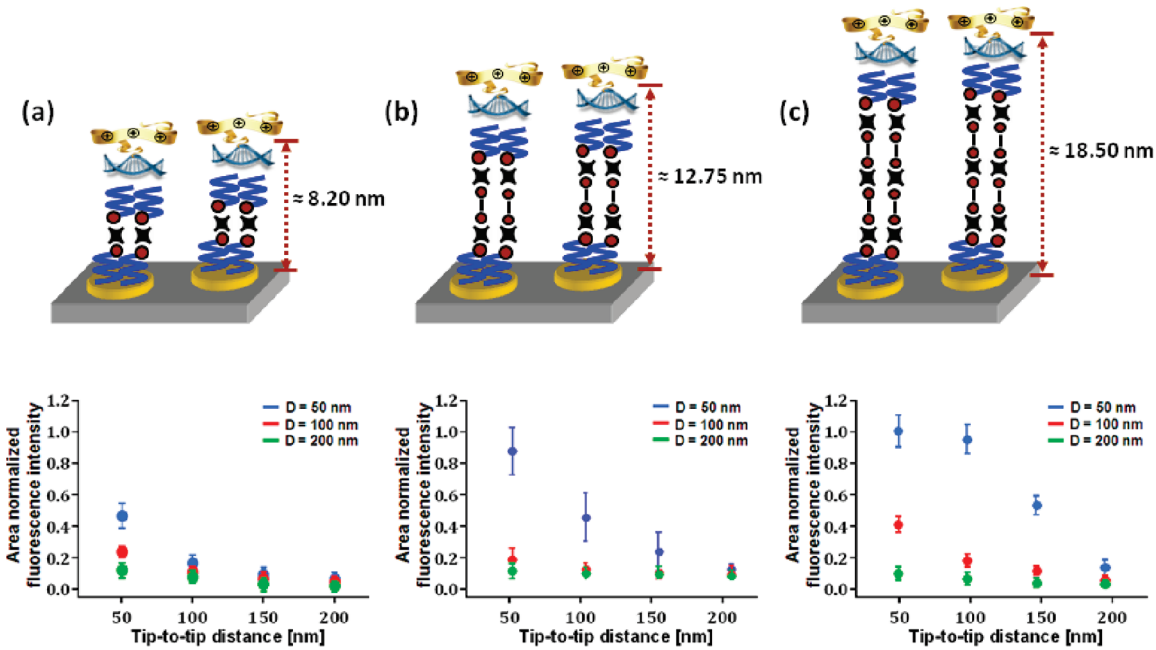

FIGURE 4. Area normalized fluorescence intensity of plasmon enhanced PFDBT-N$^+$ nanoarrays versus tip-to-tip distance (nm) at three different PFDBT-N$^+$–metal distances (a) ≈8.20 nm, (b) ≈12.75 nm, and (c) ≈18.50 nm. The diameters of the nanodisk are labeled accordingly: blue, D = 50 nm; red, D = 100 nm; and green, D = 200 nm. Schematic illustrations depict the nanoassembly of PFDBT-N$^+$ at the corresponding metal distances.

clear uniform layer. Details on the data calculations can be found in a previous publication (39a). At the three CP–metal distances, PFDBT-N$^+$ emission decreases as the tip-to-tip spacing (d_{tt}) increases. With a larger CP–metal distance of ~18.50 nm, the PFDBT-N$^+$ emission is higher than PFDBT-N$^+$ placed ~8.20 and ~12.75 nm from the metal surface and decreases thereafter when the CP–metal distance is further increased (data not shown). Stronger plasmon coupling are believed to be responsible for this observation. With small nanopillar spacings, PFDBT-N$^+$ emission intensity decreases as d_{tt} increases. On the smaller nanopillars, PFDBT-N$^+$ emission is most intense at a d_{tt} spacing of 50 nm and decreases with larger d_{tt}. Similar findings using QDs were reported where higher QD emission is observed at a QD–metal distance of ~16.0 nm (39a).

The degree of spectral overlap between the plasmon coupling of the nanoarray and PFDBT-N$^+$ emission at 640 nm was shown to affect the emission intensity of PFDBT-N$^+$. PFDBT-N$^+$ emission is higher when assembled onto nanoarrays where the d_{tt}= 50 and 100 nm. For these nanoarrays, the LSPR peaks are ranging from 600 to 675 nm and, therefore, have a higher degree of spectral overlap compared to nanoarrays where d_{tt} = 150 and 200 nm. It should be noted that changes in the refractive index (RI) of the surface of nanoparticles result in a shift of the plasmon resonance peak position. The sensitivity to the degree of

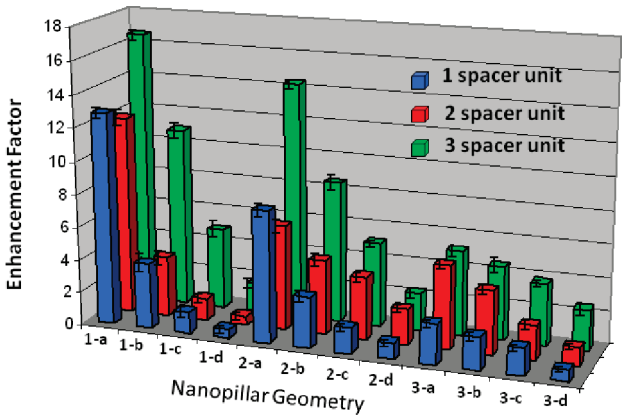

FIGURE 5. Enhancement factors of PFDBT-N$^+$ nanoarrays. The calculations were performed by dividing the fluorescence intensity of PFDBT-N$^+$ self-assembled on the gold nanoarrays by the fluorescence intensity of PFDBT-N$^+$ on the gold nanoarrays. 1 spacer unit (blue) corresponds to a PFDBT-N$^+$−metal distance of ≈8.20 nm; 2 spacer unit (red) corresponds to a PFDBT-N$^+$−metal distance of ≈12.75 nm; and 3 spacer unit (green) corresponds to PFDBT-N$^+$−metal distance of ≈18.50 nm.

LSPR shift is dependent on the shape and metal type. In particular, spherical nanoparticles exhibit smaller LSPR shifts than that of triangular nanoparticles (51), and gold nanoparticles have less spectral peak shift in response to a change in RI than silver nanoparticles (52). Thus, the plasmon resonance peak position of the modified gold nanoarray is not expected to have a large shift from the unmodified gold nanoarrays. The higher degree of spectral overlap allowed for a stronger field coupling and, therefore, higher PFDBT-N$^+$ emission.

Plasmon enhanced fluorescence of CP nanoarrays were fabricated using a layer-by-layer self assembly approach to obtain a 16-fold increase in PFDBT-N$^+$ emission. PFDBT-N$^+$ assembled on smaller nanoarrays and at a CP−metal distance of ∼18.50 nm showed the highest fluorescence enhancement. Enhancement factors were calculated relative to the emission of a spin-coated thin film of PFDBT-N$^+$ on the nanoarrays. Enhancement factors of PFDBT-N$^+$ nanoarrays are shown in Figure 5. For a given nanopillar diameter, a smaller tip-to-tip spacing (d_{tt} = 50 nm) showed higher PFDBT-N$^+$ emission due to stronger near-field coupling between neighboring nanoparticles within the array and, therefore, higher degree of spectral overlap between the plasmon resonance and PFDBT-N$^+$ emission.

CONCLUSION

In summary, a peptide-mediated layer-by-layer approach is used to assemble cationic conjugated polymers onto lithographic nanopillars and to enhance the CPs emission. The peptide-linked structures assembled PFDBT-N$^+$ on the optimum nanoarrays where a 16-fold increase in the photoluminescence of PFDBT-N$^+$ is observed. Although nanopillars are not the most appropriate shapes for highest enhancement factors, we demonstrate a proof-of-concept study on self-assembled conjugated polymer structures. Other nanostructures will be fabricated and studied in due course. This enhanced CP emission from the assembly of CP nanoarrays shows spectral overlap and CP−metal distance can be used to enable precise control for the development of multifunctional nanomaterials for biotechnology.

Acknowledgment. The authors thank the support from the National Science Foundation's NSF-STC program and GEMSEC (Genetically Engineered Materials Science and Engineering Center) through the NSF-MRSEC program and the World Class University (WCU) program through the National Research Foundation of Korea under the Ministry of Education, Science, and Technology (R31-10035). A.K.-Y.J. thanks the Boeing-Johnson Foundation for financial support. Instrumentation for electron-beam lithography was provided by the Nanotechnology User Facility (NTUF), a member of the National Nanotechnology Infrastructure (NNIN) supported by NSF.

Supporting Information Available: Experimental procedure on the layer-by-layer assembly of PFDBT-N$^+$ on gold nanoarrays and on flat gold substrates for linker height measurement, characterization of peptide and biotin-SA linkers, and AFM measurement of linker lengths. This material is available free of charge via the Internet at http://pubs.acs.org.

REFERENCES AND NOTES

(1) Maier, S. A.; Kik, P. G.; Atwater, H. A.; Meltzer, S.; Harel, E.; Koel, B. E.; Requicha, A. A. G. *Nat. Mater.* **2003**, *2*, 229–232.
(2) Griep, M.; Winder, E.; Lueking, D.; Friedrich, C.; Mallick, G.; Karna, S. *J. Nanosci. Nanotechnol.* **2010**, *10*, 6029–6035.
(3) Hess, H.; Bachand, G. D.; Vogel, V. *Chem.—Eur. J.* **2004**, *10*, 3220–2116.
(4) Ruiz-Hitzky, E.; Ariga, K.; Lvov, Y. M. In *Bio-inorganic hybrid nanomaterials: Strategies, Synthesis, Characterization, and Applications*; Wiley-VCH: New York, 2008.
(5) Darder, M.; Arandan, P.; Ruiz-Hitzky, E. *Adv. Mater* **2007**, *19*, 1309–1319.
(6) Salata, O. *J. Nanobiotechnol.* **2004**, *2*, 1–6.
(7) Tamerler, C.; Sarikaya, M. *ACS Nano* **2009**, *3*, 1606–1615.
(8) (a) Hau, S. K.; Yip, H.-L.; Leong, K.; Jen, A. K-Y. *Org. Electron.* **2009**, *10*, 719–723. (b) Westphalen, M.; Kreibig, U.; Rostalski, J.; Luth, H.; Meissner, D. *Sol. Energy Mater. Sol. Cells* **2000**, *61*, 97–105.
(9) (a) Haes, A. J.; Hall, W. P.; Chang, L.; Klein, W. L.; Van Duyne, R. P. *Nano Lett.* **2004**, *4*, 1029–1034. (b) Haes, A. J.; Van Duyne, R. P. *J. Am. Chem. Soc.* **2002**, *124*, 10596–10604. (c) Haes, A. J.; Zou, S.; Schatz, G. C.; Van Duyne, R. P. *J. Phys. Chem. B* **2004**, *108*, 6961–6968. (d) Elghanian, R.; Storhoff, J. J.; Mucic, R. C.; Letsinger, R. L.; Mirkin, C. A. *Science* **1997**, *277*, 1078–1080. (e) Bruchez, M., Jr.; Moronne, M.; Gin, P.; Weiss, S.; Alivisatos, A. P. *Science* **1998**, *281*, 2013–2016. (f) Medintz, I. L; Uyeda, H. T.; Goldman, E. R.; Mattoussi, H. *Nat. Mater.* **2005**, *4*, 435–446.
(10) (a) Chowdhury, M. H.; Ray, K.; Gray, S. K.; Pond, J.; Lakowicz, J. R. *Anal. Chem.* **2009**, *81*, 1397–1403. (b) Huang, X.; El-Sayed, I. H.; Qian, W.; El-Sayed, M. A. *J. Am. Chem. Soc.* **2006**, *128*, 2115–2120. (c) Nie, S.; Emory, S. R. *Science* **1997**, *275*, 1102–1106. (d) Hirsch, L. R.; Stafford, R. J.; Bankson, J. A.; Sershen, S. R.; Rivera, B.; Price, R. E.; Hazle, J. D.; Halas, N. J.; West, J. L. *Proc. Natl. Acad. Sci. U.S.A.* **2003**, *100*, 13549–13554. (e) Jain, P. K.; El-Sayed, I. H.; El-Sayed, M. A. *Nano Today* **2007**, *2*, 18–29.
(11) Willner, I.; Willner, B. *Nano Lett.* **2010**, in press.
(12) Chen, Y.; Munechika, K.; Jen-La Plante, I.; Munro, A. M.; Skrabalak, S. E.; Xia, Y.; Ginger, D. S. *Appl. Phys. Lett.* **2008**, *93*, 053106–053112.
(13) Anger, P.; Bharadwaj, P.; Novotny, L. *Phys. Rev. Lett.* **2006**, *96*, 113002–113004.
(14) (a) McQuade, D. T.; Pullen, A. E.; Swager, T. M. *Chem. Rev.* **2000**, *100*, 2537–2574. (b) Wang, Y.; Liu, B. *Biosens. Bioelectron.* **2009**, *24*, 3293–3298.
(15) Yu, J.; Wu, C.; Sahu, S. P.; Fernando, L. P.; Szymanski, C.; McNeill, J. *J. Am. Chem. Soc.* **2009**, *51*, 18410–18414.

(16) Di Benedetto, F.; Camposeo, A.; Pagliara, S.; Mele, E.; Persano, L.; Stabile, R.; Cingolani, R.; Pisignano, D. *Nat. Nanotechnol.* **2008**, *3*, 614–619.
(17) Green, M.; Howes, P.; Berry, C.; Argyros, O.; Thanou, M. *Proc. R. Soc. A* **2009**, *465*, 2751–2759.
(18) Baier, M. C.; Huber, J.; Mecking, S. *J. Am. Chem. Soc.* **2009**, *131*, 14267–14273.
(19) Chen, L.; McBranch, D. W.; Wang, H.-L.; Helgeson, R.; Wudl, F.; Whitten, D. G. *Proc. Natl Acad. Sci. U.S.A.* **1999**, *96*, 12287–12292.
(20) Lee, K.; Povlich, L. K.; Kim, J. *Adv. Funct. Mater.* **2007**, *17*, 2580–2587.
(21) Dogariu, A.; Gupta, R.; Heeger, A. J.; Wang, H. *Synth. Met.* **1999**, *100*, 95–100.
(22) Moliton, A.; Hiorns, R. C. *Polym. Int.* **2004**, *53*, 1397–1412.
(23) (a) Achyuthan, K. E.; Bergstedt, T. S.; Chen, L.; Jones, R. M.; Kumaraswamy, S.; Kushon, S. A.; Ley, K. D.; Lu, L.; McBranch, D.; Mukundan, H.; Rininsland, F.; Shi, X.; Xia, W.; Whitten, D.G. *J. Mater. Chem.* **2005**, *15*, 2648–2565. (b) Liu, B.; Bazan, G. C. *J. Am. Chem. Soc.* **2004**, *126*, 1942–1943.
(24) Ho, H. A.; Dorè, K.; Boissinot, M.; Bergeron, M. G.; Tanguay, R. M.; Boudreau, D.; Leclerc, M. *J. Am. Chem. Soc.* **2005**, *127*, 12673–12676.
(25) (a) Heeger, P. S.; Heeger, A. J. *Proc. Natl. Acad. Sci. U.S.A.* **1999**, *96*, 12219–12221. (b) Peter, K.; Nilsoon, R.; Ingalis, O. *Nat. Mater.* **2003**, *2*, 419–424. (c) Ho, H.-A.; Boissinot, M.; Bergeron, M. G.; Corbeil, G.; Dorè, K.; Boudreau, D.; Leclerc, M. *Angew. Chem.* **2002**, *114*, 1618–1621. (d) Haskins-Glusac, K.; Pinto, M. R.; Tan, C.; Schanze, K. S. *J. Am. Chem. Soc.* **2004**, *126*, 14964–14971. (e) Pun, C. C.; Lee, K.; Kim, H.-J.; Kim, J. *Macromolecules* **2006**, *39*, 7461–7463.
(26) Liu, B.; Bazan., G. C. *Proc. Natl. Acad. Sci. U.S.A.* **2005**, *102*, 589–593.
(27) Gaylord, B. S.; Heeger, A. J.; Bazan, G. C. *Proc. Natl. Acad. Sci. U.S.A.* **2002**, *99*, 10954–10957.
(28) Baker, E.S.; Hong, J. W.; Gaylord, B. S.; Bazan, G. C.; Bowers, M. T. *J. Am. Chem. Soc.* **2006**, *128*, 8484–8492.
(29) Ho, H.-A.; Najari, A.; Leclerc, M. *Acc. Chem. Res.* **2008**, *41*, 168–178.
(30) Munechika, K.; Chen, Y.; Tillack, A.; Kulkarni, A. P.; Jen-La Plante, I.; Murno, A. M.; Ginger, D. S. *Nano Lett.* **2010**, *10*, 2598–2603.
(31) Yang, B.; Lu, N.; Qi, D.; Ma, R.; Wu, Q.; Hao, J.; Liu, X.; Mu, Y.; Reboud, V.; Kehagias, N.; Sotomayor Torres, C. M.; Boey, F. Y. C.; Chen, X.; Chi, L. *Small* **2010**, *6*, 1038–1043.
(32) Lakowicz, J. R. In *Principles of Fluorescence Spectroscopy*, 3rd ed.; Kluwer Academic/Plenum Publishers: New York, 2006.
(33) Aslan, K.; Gryczynski, I.; Malicka, J.; Matveeva, R.; Lakowicz, J. R.; Geddes, C. D. *Curr. Opin. Biotechnol.* **2005**, *16*, 55–62.
(34) Sabanayagam, C. R.; Lakowicz, J. R. *Nucl. Acids Res.* **2006**, *35*, 1–9.
(35) Geddes, C. D.; Gryczynski, I.; Malicka, J.; Gryczynski, Z.; Lakowicz, J. R. *Comb. Chem. High Throughput Screening* **2003**, *6*, 109–117.
(36) Cho, C.-Y.; Kwon, M.-K.; Lee, S.-J.; Han, S.-H.; Kang, J.-W.; Kang, S.-E.; Lee, D.-Y.; Park, S.-J. *Nanotechnology* **2010**, *21*, 205201. (5 pp).
(37) Geddes, C. D.; Lakowicz, J. R. *J. Fluoresc.* **2002**, *12*, 121–129.
(38) Kelly, K. L.; Coronado, E.; Zhao, L. L.; Schatz, G. C. *J. Phys. Chem. B* **2003**, *107*, 668–677.
(39) (a) Zin, M. T.; Leong, K.; Wong, N.-G.; Ma, H.; Sarikaya, M.; Jen, A. K.-Y. *Nanotechnology* **2009**, *20*, 015305. (b) Pompa, P. P.; Martiradonna, L.; Della Torre, A.; Carbone, L.; del Mercato, L. L.; Manna, L.; De Vittorio, M.; Calabi, F.; Cingolani, R.; Rinaldi, R. *Sens. Actuators, B* **2007**, *126*, 187. (c) Gopinath, A.; Boriskina, S. V.; Reinhard, B. M.; Dal Negro, L. *Opt. Express* **2009**, *17*, 3741–3753.
(40) (a) Kneipp, K.; Wang, Y.; Kneipp, H.; Perelman, L. T.; Itzkan, I.; Dasari, R. R.; Feld, M. S. *Phys. Rev. Lett.* **1997**, *78*, 1667–1670. (b) Xu, H. X.; Bjerneld, E. J.; Kall, M.; Borjesson, L. *Phys. Rev. Lett.* **1999**, *83*, 4357–4360. (c) Michaels, A. M.; Nirmal, M.; Brus, L. E. *J. Am. Chem. Soc.* **1999**, *121*, 9932–9939. (d) Jackson, J. B.; Halas, N. J. *Proc. Natl. Acad. Sci. U.S.A.* **2004**, *101*, 17930–17935.
(41) Hao, E.; Li, S.; Bailey, R. C.; Zou, Z.; Schatz, G.C.; Hupp, J. T. *J. Phys. Chem. B* **2004**, *108*, 1224.
(42) Pompa, P. P.; Martiradonna, L.; Della Torre, A.; Della Sala, F.; Manna, L.; De Vittorio, M.; Calabi, F.; Cingolani, R.; Rinaldi, R. *Nat. Nanotechnol.* **2006**, *1*, 126.
(43) Shankar, S. S.; Rizzello, L.; Cingolani, R.; Rinaldi, R.; Pompa, P. P. *ACS Nano* **2009**, *3*, 893–900.
(44) Zhang, J.; Malicka, J.; Gryczynski, I.; Lakowicz, J. R. *J. Phys. Chem. B* **2005**, *109*, 7643.
(45) (a) Huang, F.; Hou, L.; Shen, H.; Jiang, J.; Wang, F.; Zhen, H.; Cao, Y. *J. Mater. Chem* **2005**, *15*, 2499–2507. (b) Yang, R. Q.; Wu, H. B.; Cao, Y.; Bazan, G. C. *J. Am. Chem. Soc.* **2006**, *128*, 14422–14423.
(46) Hnilova, M.; Oren, E. E.; Seker, U. O. S.; Wilson, B.; Collino, S.; Evans, J. S.; Tamerler, C.; Sarikaya, M. *Langmuir* **2008**, *24*, 12440.
(47) Yang, Y.; Matsubara, S.; Nogami, M.; Shi, J.; Huang, W. *Nanotechnology* **2006**, *17*, 2821–2827.
(48) Leong, K.; Chen, Y.; Masiello, D. J.; Zin, M. T.; Hnilova., M.; Ma, H.; Tamerler, C.; Sarikaya, M.; Ginger, D. S.; Jen, A. K-Y. *Adv. Funct. Mater* **2010**, *20*, 2675–2682.
(49) Sarikaya, M.; Tamerler, C.; Schuten, K.; Jen, A. K-Y.; Baneyx, F. *Nat. Mater.* **2003**, *2*, 577.
(50) Gaylord, B. S.; Heeger, A. J.; Bazan, G. C. *Proc. Natl. Acad. Sci. U.S.A.* **2002**, *99*, 10954–10957.
(51) Takahashi, Y.; Tatsuma, T. *Nanoscale* **2010**, *2*, 1494–1499.
(52) Mock, J. J.; Smith, D. R.; Schultz, S. *Nano Lett.* **2003**, *3*, 485–491.

AM100635V